

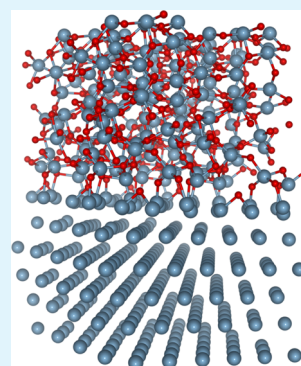
Oxidation Protection with Amorphous Surface Oxides: Thermodynamic Insights from Ab Initio Simulations on Aluminum

Muratahan Aykol^{†,§} and Kristin A. Persson^{*,†,‡}

[†]Energy Storage and Distributed Resources Division, Lawrence Berkeley National Laboratory, Berkeley, California 94720, United States

[‡]Department of Materials Science, University of California Berkeley, Berkeley, California 94720, United States

ABSTRACT: Native surface films play a key role in the oxidation and corrosion protection of functional and structural materials. Here, we present a fully ab initio approach for understanding the thermodynamic driving force behind the initial phase selection among amorphous and crystalline structures for a surface film growing on a crystalline substrate. We apply the approach to elucidate the competition among corundum (α), spinel (γ), and amorphous (am.) Al_2O_3 films growing on aluminum metal. We show that the amorphous Al_2O_3 film becomes thermodynamically the most stable form below around ~ 1 nm, that is, the relative energetic stabilities of thin polymorphic Al_2O_3 films follow $\text{am.} < \gamma < \alpha$. As the film thickness increases, the relative stability relation first changes to $\gamma < \alpha < \text{am.}$ and then to the bulk limit of $\alpha < \gamma < \text{am.}$ The nanoscale γ films distort substantially to form exclusively four- and fivefold-coordinated Al–O polyhedra, lose the close-packed O framework, and become “amorphous-like”, that is, exhibit both short-range order and energetic characteristics that are commensurate with the amorphous form. Our results provide a quantitative, first-principles confirmation for the early hypotheses on the thermodynamic stability of amorphous surface films and provide insights for the critical role they play in oxidation protection. Handling the complexities associated with the initial film growth, including bulk, surface, interface, and strain energy effects in realistically complex ab initio simulations, we expect this approach to contribute to understanding of the mechanism behind effective passivation films for aluminum alloys and beyond.



KEYWORDS: surface films, polymorph selection, amorphous films, oxidation, corrosion, thin-film growth, aluminum

1. INTRODUCTION

Passivation of metals or semiconductors enabled by the formation of a thin protective film, such as a native oxide on the surface, has enabled many major technological advances.¹ However, after decades of research, the formation and functionality of passivation films are still not entirely understood.^{1,2} The growth and breakdown of passivation films have been studied with a range of phenomenological models including but not limited to the Verwey, Cabrera–Mott, and point-defect models,³ which aim at explaining the evolution of an existing passivation film.¹ Structural, bulk thermodynamic (e.g., Pourbaix diagrams), electronic, and kinetic aspects of passivation layers at steady state are all extensively studied.⁴ The thermodynamic requirements for the formation of the very first, atomic-scale oxide layer with a protective nature, however, are rarely addressed quantitatively because of the complex interplay between the bulk, surface, and interfacial degrees of freedom at such length scales.

Starting with early microscopy and diffraction experiments, evidence has culminated in the literature demonstrating that in systems resistant to corrosion or low-temperature oxidation, such as Al, Cr, Ta, Fe–Cr, and Si, native surface films tend to have a uniform amorphous morphology, especially during the onset of film formation.^{5–13} For example, increasing the Cr content in Fe–Cr alloys results in a transition from a less-protective crystalline oxide overgrowth to an amorphous, more

protective one above a threshold Cr content of approximately 15%, which has been argued to be a primary mechanism underlying the corrosion resistance of stainless steels.^{8,14–16} Aluminum is one of the earliest known examples where a native amorphous oxide was shown to grow on the metal surface and claimed to provide effective low-temperature oxidation protection.^{5–7,17–21}

The effectiveness of amorphous films as passivation layers is associated with the lack of grain boundaries, dislocations, or other highly defective regions that exist in polycrystalline films which would enhance the kinetics of metal and/or oxygen ion transport.^{10,22} Although bulk diffusion in polycrystalline oxides can be slow, such defective regions may facilitate orders of magnitude faster diffusion^{23,24} and therefore deteriorate the effectiveness of the film. Besides, nucleation of crystalline films is strongly influenced by epitaxial relations, and thus, such films may not provide a homogenous, uniform surface coverage and lead to patchy regions and chipping, exposing the metal substrate, for example, as in iron, as empirically addressed often using the Pilling–Bedworth ratio.²⁵ Amorphous films, on the other hand, tend to be conformal¹⁷ because of their isotropic nature (lack of a preferred epitaxy and strain energy) as well as

Received: September 29, 2017

Accepted: January 3, 2018

Published: January 3, 2018

smaller interface and surface energies. If such films can provide sufficiently slow cation diffusion out of the film or anion diffusion into the film, they can effectively suppress corrosion.^{7,10,11} Formation of an amorphous film on a substrate was long thought to be a kinetic phenomenon, and such passivation films were assumed to be in a metastable state. Later, Jeurgens et al.²⁶ and Reichel et al.²⁷ developed an empirical thermodynamic framework to understand the stability of the amorphous films with respect to crystal overgrowths on various metal substrates including Al, Fe, Cu, Zn, and Mg and showed that an amorphous film can in fact become the thermodynamically preferred morphology at small length scales in certain systems.

The thermodynamics of systems describing the amorphous or crystalline film growing on a substrate involves many degrees of freedom associated with the surfaces and interfaces (planes, terminations, epitaxial relations, reconstructions, etc.), strain effects, and bulk energies of competing amorphous and crystalline polymorphs. More importantly, as the films get thinner (nanometer or subnanometer scale), the energetic contributions are highly entangled and may not be linearly separable, such that projections from separate calculations of surface, interface, and bulk energetics are not guaranteed to be descriptive. Given the significant increase in computational power in recent years, we suggest that a strategy to overcome these limitations in predictive modeling of surface overgrowths is building realistically complex, “all-inclusive” *ab initio* simulations that capture the actual substrate–film morphology. In this work, we present such a framework that combines large-scale *ab initio* molecular dynamics (AIMD) and density functional theory (DFT) calculations of crystalline and amorphous Al₂O₃ films on a face-centered cubic, fcc (111) aluminum substrate. We provide first-principles evidence for the thermodynamic stabilization of the amorphous aluminum oxide film over other crystalline alumina polymorphs at the nanoscale on the Al metal. We propose that the computational framework presented here for aluminum can be broadly applicable to understand and craft materials–design strategies for inducing native, effective passivation films in more complex alloy systems and for the synthesis of thin films.

2. MODEL GENERATION AND COMPUTATIONAL METHODS

2.1. Generation of Model Structures. **2.1.1. Preparation of the Al Substrate.** To properly accommodate an isotropic amorphous film on an aluminum substrate, we constructed (111) Al slabs in an orthorhombic supercell, with in-plane (*a* and *b*) dimensions ([111] and [221] directions, respectively) that are sufficiently large and similar in magnitude. The *a* and *b* directions need to be long enough to ensure that there exists enough space above the substrate for a representative amorphous film to be inserted. As pairwise correlations in amorphous Al₂O₃ vanish within approximately 5 to 8 Å for all pairs,²⁸ we found that an orthorhombic (111) Al slab configuration with *a* = 8.568 Å and *b* = 9.893 Å is sufficiently large to accommodate a representative amorphous film above, without inducing significant artificial correlation across the periodic boundaries for the film. In the orthogonal (*c*) direction, the metal substrate is composed of 6 (111) layers of fcc Al, which yields a 72-atom slab with a thickness of 11.660 Å. This slab thickness is sufficiently large and is in line with similar studies of metal substrates.²⁹ The height of the simulation cell in the *c*-direction is fixed at ~50 Å, providing a large vacuum of at least 20 Å when amorphous or crystalline films are inserted above the Al substrate. The dimensions of the supercells above are derived from the lattice constant of bulk Al (4.039 Å), as obtained from the Materials Project database.³⁰ In all substrate–film calculations, the positions of

the Al atoms in the two middle layers of the Al slab are fixed to mimic the bulk region, whereas two layers near the surface on both sides of the slab are allowed to fully relax.

2.1.2. Preparation of Amorphous Film/Al Substrate Configurations. For the amorphous surface films, we start by creating an Al₂O₃ liquid using AIMD in an orthorhombic box that has the same *a* and *b* dimensions as the Al substrate described above, and the *c*-dimension is adjusted to yield a liquid density that is ~15% larger than that of α -Al₂O₃, which, in our experience, provides sufficient amount of free volume for fast equilibration of the melt while avoiding any possible void formation. As the *a* and *b* dimensions match the substrate, this process ensures that any subsequent amorphous film derived from the liquid does not develop artificial strains when transferred onto the Al substrate. We run an AIMD simulation in the *NVT* ensemble for the liquid corresponding to the thickest amorphous film considered (120 atoms) at 4000 K for 5000 molecular dynamics (MD) steps, with a 2 fs time step. In the second (production) stage, the liquid is simulated for an additional 5000 MD steps, from which five independent isochronal configurations are selected. These selected configurations are then transferred on to the (111) Al slab, utilizing their existing atomic arrangements near the boundaries of their initial simulation box as interfaces/surfaces in the new substrate–film system. This process is equivalent to cleaving the bulk amorphous configurations at a random position to create an interface with Al and an oxide surface. Hence, at this stage, the positional degrees of freedom of atoms near the substrate–film interface, film surface, and in the bulk of the film need to be further optimized to find the nearby local minima on the potential energy landscape. Keeping the positions of the mid-layer Al atoms fixed as described above, we perform an additional 1000-step AIMD run in this substrate–film cell (192 atoms: 72 atoms in Al substrate + 120 atoms in Al₂O₃ film) at a moderate temperature of 600 K. This procedure allows sufficiently fast kinetics for the effective relaxation and reconstruction of both the amorphous film/Al substrate interfaces and the film surface, without introducing any significant changes to the bulk of the amorphous film or the crystalline substrate. A subsequent, higher-precision DFT-based conjugate-gradient structure optimization is performed at the end of this MD optimization to obtain the final energies of the 192-atom supercells. Thinner films are obtained by removing stoichiometric portions of Al₂O₃ from the top of the films and repeating the AIMD + DFT optimization routine described above. For each film thickness, the configuration that yields the lowest energy is selected for further stability comparisons.

2.1.3. Preparation of Corundum Film/Al Substrate Configurations. There exists a relatively low-strain epitaxial relation between the (111) Al substrate and the (0001) plane in the hexagonal α -Al₂O₃,^{29,31} with [10 $\bar{1}0$] direction parallel to $\bar{1}10$ of fcc Al. With the lattice parameters of these phases acquired from the Materials Project,³⁰ we found that the strains in each orthogonal direction are both ~3% for α -Al₂O₃ when the film is strained to match the Al substrate. We tested the α -Al₂O₃ substrate with both Al and O terminations of the (0001) plane.

2.1.4. Preparation of Gamma Alumina Film/Al Substrate Configurations. γ -Al₂O₃ adopts a spinel structure where it ideally has a 3:4 ratio of metal and oxygen sites, and the metal sites themselves have a 1:2 ratio of the tetrahedral and octahedral coordination sites. Therefore, to satisfy the γ -Al₂O₃ stoichiometry, deviating from the chemical formula of a spinel, M₃O₄ (M = a metal or mixed metals), the Al atomic positions are not fully occupied. Configurations of such vacancies have been extensively studied in literature but are still not well-known.^{32–34} DFT calculations consistently indicate that these octahedral vacancies yield more stable structures than the tetrahedral or mixed octahedral/tetrahedral vacancy configurations.^{33,34} Here, we adopt the vacancy configuration introduced by Pinto et al.,³⁴ where two octahedral Al vacancies were introduced into the 14-atom rhombohedral spinel unit cell. Assuming this structure, we determined 12 unique ways to cleave γ -Al₂O₃ in the close-packed (111) plane (for the standard spinel unit cell). Because of the close-packed O framework in the spinel structure, there is a natural epitaxial relation between the (111) planes in Al and γ -Al₂O₃, as known from the oxidation experiments of Al.^{17,35} Straining the γ -Al₂O₃

substrate from the calculated $a = b = 5.663 \text{ \AA}$ to that of Al at the 2×2 (111) Al substrate yields a small linear strain of $\sim 0.8\%$ in both directions. Among the 12 ways of cleaving $\gamma\text{-Al}_2\text{O}_3$ in the (111) plane, four structures were found to have surface terminations through the introduced vacancies and therefore are chosen to further study with first-principles, as they are the most likely candidates for energetically favorable surface and interface configurations.³⁴ These four possible terminations yield slabs that are not symmetrical, meaning either side of the slab can be interfaced with the Al substrate. Therefore, we test eight unique $\gamma\text{-Al}_2\text{O}_3$ film/Al substrate configurations.

For both α and γ film systems, to allow possible reconstructions and accelerate the optimization of atomic positions near surfaces and interfaces, we follow the same AIMD + DFT optimization procedure described above for the amorphous film. The procedure is repeated for thinner films after removing stoichiometric amounts of Al_2O_3 from the top of the films. The lowest-energy configurations of alumina film/Al substrate systems for α , γ , and amorphous alumina at different film thicknesses are illustrated in Figure 1.

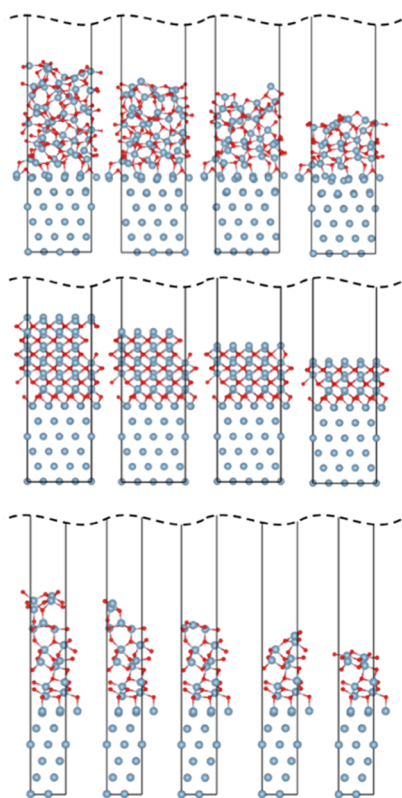


Figure 1. Morphologies of Al metal substrates with amorphous Al_2O_3 (top), $\alpha\text{-Al}_2\text{O}_3$ (middle), and $\gamma\text{-Al}_2\text{O}_3$ (bottom) films of varying amounts after structure optimization.

2.2. DFT and AIMD Calculations. All first-principles calculations were performed using the Vienna Ab initio Simulation Package.^{36,37} The Perdew–Burke–Ernzerhof formulation³⁸ of the generalized gradient approximation functional is used with projector-augmented wave potentials³⁹ at a plane-wave kinetic-energy cutoff of 520 eV in the structure-optimization calculations. In all such calculations, we consistently use a relatively dense k -point mesh of $4 \times 4 \times 2$ for the supercells described above. For computational efficiency, we use relatively low-precision settings with Γ -point only Brillouin zone integration at a plane-wave kinetic-energy cutoff of 400 eV in AIMD simulations. The computational workflows for AIMD and DFT calculations of amorphous and crystalline structures and substrate–film systems involved the pymatgen,⁴⁰ custodian,⁴⁰ fireworks,⁴¹ and atomate⁴² codes and can be found as part of the open-source mpmorph package at <http://github.com/materialsproject/mpmorph>. Structures were visualized with VESTA.⁴³

3. RESULTS AND DISCUSSION

The structure and composition of oxide overgrowths critically control their thermodynamic properties. We note that the composition of thin-film overgrowths may deviate from their bulk stoichiometry depending on factors such as the substrate metal's surface orientation, temperature, pressure, and oxygen chemical potential.^{21,44,45} In the case of low-temperature oxidation of aluminum metal, recent angle-resolved X-ray photoelectron spectroscopy measurements indicate that the O/Al ratio in the amorphous oxide overgrowth is close to 1.5.⁴⁴ In terms of the structure, the framework we present allows for the relaxation and reconstruction of interfaces and surfaces in the substrate–film systems with an intermediate AIMD step; however, the bulk of the amorphous film as obtained via a melt-quench route still serves as an approximation to the amorphous structure that would result from a surface reaction of aluminum with oxygen. The first-peak positions of the RDFs of the amorphous Al_2O_3 structures generated in this work (Figure 2) are ~ 0.18 , ~ 0.28 , and ~ 0.32 nm for the Al–O, O–

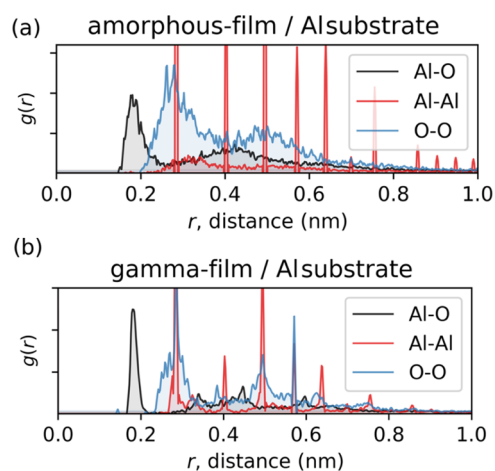


Figure 2. Radial distribution functions (RDFs), $g(r)$, for (a) amorphous Al_2O_3 film/Al substrate and (b) $\gamma\text{-Al}_2\text{O}_3$ film/Al substrate. Sharp Al–Al peaks correspond to the metal substrate. Note, here, that the normalization of $g(r)$ functions is nonstandard (i.e., not converging to unity at large separations) as these are calculated in the film–substrate supercells.

O, and Al–Al pairs, respectively. This is in good agreement with RDFs derived from X-ray and neutron diffraction of anodically oxidized aluminum foils by Lamparter and Kniep.²⁸ Moreover, the distribution of the local polyhedral units AlO_n (Al coordinated with n O atoms) of amorphous alumina films in this work (Figure 3) and the resulting average Al–O coordination number of ~ 4.2 are also similar to the findings in the same experimental report. Overall, these results indicate that the stoichiometric Al_2O_3 films generated here with a framework that involves a melt-quench route do provide a reasonable structural and compositional approximation for the actual amorphous alumina overgrowths on aluminum.

For the $\alpha\text{-Al}_2\text{O}_3$ /Al film, the configuration with the O-terminated side of the film interfacing the Al substrate and Al-terminated side of the film forming the surface is found to be lower in energy (by ~ 60 meV/atom) than the film aligned in the opposite way with the substrate. The relaxation of the $\alpha\text{-Al}_2\text{O}_3$ films compared to the bulk α is not significant, and the crystalline framework is preserved even for the thinnest film. On the other hand, as evident in Figure 1, the lowest-energy γ

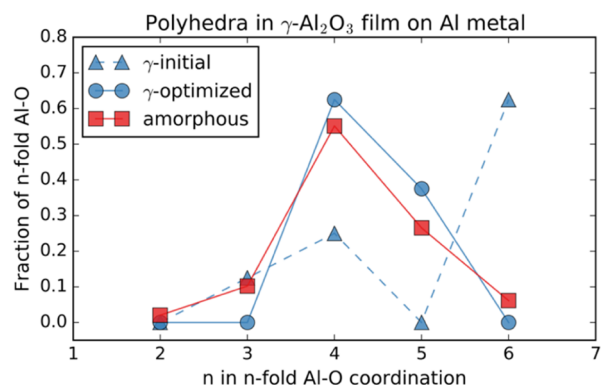


Figure 3. Change in the Al–O coordination environment in the (0001) γ - Al_2O_3 film on the (111) Al substrate for the lowest-energy (sixth) configuration in Figure 4.

film is significantly distorted despite the low lattice mismatch with the Al substrate. In fact, a visual inspection of the initial and relaxed structures of the eight different γ - Al_2O_3 /Al substrate configurations indicates that most γ films experience a significant distortion of the spinel framework during the relaxation regardless of their relative stabilities as shown in Figure 4. The distribution of local coordinations before and after relaxation in Figure 3 indicates that no sixfold O-coordinated Al remain in the γ film, instead four- and fivefold-coordinated Al atoms dominate the film structure. Interestingly, the distribution of Al–O coordination in the γ film approaches that of the amorphous film. The RDFs of amorphous Al_2O_3 /Al substrate and γ - Al_2O_3 /Al substrate configurations in Figure 2a,b further show the loss of crystallinity in the γ film and its structural resemblance to that of the amorphous one.

The relative stabilities of (0001)- α , (111)- γ , and amorphous Al_2O_3 films on (111) Al metal substrate as a function of film thickness are shown in Figure 5, along with the respective bulk counterparts. The order of low-temperature energetic stability of bulk phases, $\alpha < \gamma < \text{am.}$, as well as the relative energies agree well with the experiments.⁴⁶ In particular, we found that the γ -alumina model structure adapted from Pinto et al.,³⁴ which has the spinel structure with the close-packed O framework and Al vacancies on octahedral sites, is 42 meV/atom above the ground-state α -alumina, close to that derived from experimental formation energies,⁴⁶ and therefore provides an accurate representation of the γ phase. The energies of the amorphous

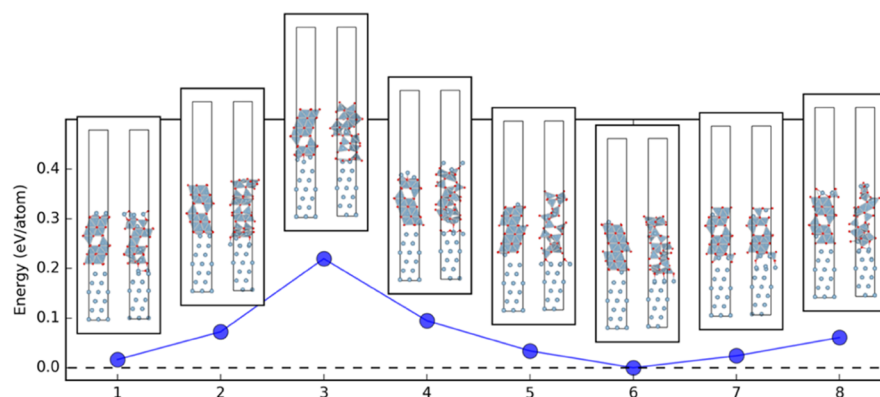


Figure 4. Relative energies and morphologies of γ - Al_2O_3 films on (111) Al substrate after structure optimization. From four unique terminations of (0001) γ - Al_2O_3 , eight different Al substrate/ γ - Al_2O_3 film combinations were obtained. Insets: film/substrate structures before (left) and after (right) relaxation for each configuration. Al–O coordinations in the films are visualized as polyhedra to show the distortions after relaxation more clearly.

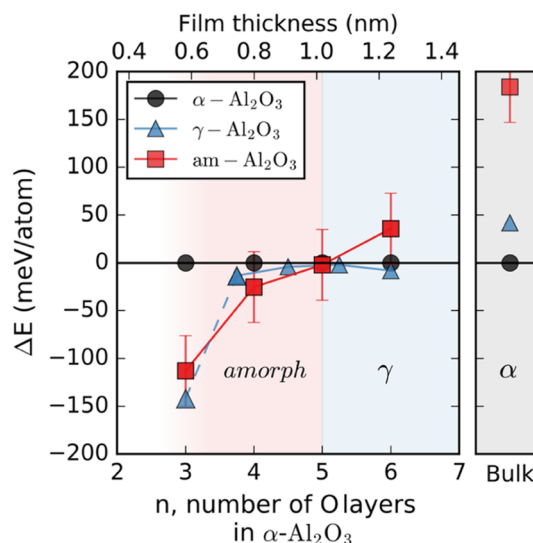


Figure 5. Energy, ΔE , of am- Al_2O_3 and (111) γ - Al_2O_3 derived films with respect to the (0001) α - Al_2O_3 film as a function of film thickness, on a (111) Al metal substrate, all calculated from first-principles. Number of O layers on the bottom horizontal-axis corresponds to number of (0001) O layers in α - Al_2O_3 film, and the corresponding approximate thickness is shown on top. Shaded regions differentiate stability regions of the films as labeled. Energy is given per atom of the oxide film. The error bars on amorphous data points show the 2σ range obtained from 10 independent bulk amorphous configurations generated. When calculating the relative energies, α - Al_2O_3 /Al energies were fit to a second-order polynomial so that the relative energies corresponding to intermediate γ - Al_2O_3 /Al configurations can be estimated.

configurations sampled are about 180 meV/atom above α -alumina and have a sample standard deviation (σ) of about 17 meV/atom.

The order of stability of alumina polymorphs growing on Al changes considerably relative to the bulk at finite length scales, as shown in Figure 5. In films with a thickness of ~ 1.0 nm and below, the amorphous Al_2O_3 film becomes more stable compared to both α and γ phases. Interestingly, around 0.6 nm (the thinnest films we studied), the γ film becomes slightly more stable than the amorphous form, but still within 2σ (~ 35 meV/atom) of the amorphous energies, implying that amorphous films at this scale are still likely to be more stable

at finite temperatures because of the entropy effects. However, due to extensive distortions in γ films discussed above, these γ films are in fact morphologically closer to the amorphous form, than to the γ form, and should be considered “amorphous-like”, explaining why the energies of amorphous and “ γ ” films at subnanometer scales on Al substrate are very close. Such film morphologies in-between amorphous and γ -alumina were in fact observed in experiments,¹⁷ and MD simulations revealed structural similarities between γ -alumina surfaces and the amorphous alumina.⁴⁷ The most likely cause of these distortions is the elimination of Al vacancies, inherently present in γ -alumina, at the film/substrate interface and surface which is facilitated further in thinner films, as compared to thicker films. We observe that for the thickest films of ~ 1.2 nm we studied, γ is slightly more stable than α . At this thickness, amorphous alumina is also still significantly more stable compared to its bulk stability, at only ~ 40 meV/atom above α . Therefore, the amorphous alumina films on aluminum are not “kinetically-trapped” phases but in fact thermodynamically compete with α and γ and can even become the ground-state film structure.

Below the “critical” thermodynamic thickness of ~ 1 nm in Figure 5, the amorphous form is not only kinetically but also thermodynamically stabilized, and therefore crystallization of γ is prohibited.^{26,27} The “limiting” thickness, on the other hand, is where the film growth becomes kinetically hindered because of slow ionic transport; for example, as predicted by the Cabrera–Mott model⁷ and as observed upon low-temperature oxidation of the aluminum. The experimental and computational reports for the limiting thickness of amorphous alumina film on Al range from ~ 0.4 to ~ 4 nm,^{17,21,48,49} under conditions with varying temperature, oxygen partial pressure, and Al surface orientation.^{50,51} The limiting thickness can be close to (as in the present case⁴⁴) but is not necessarily the same as the critical thickness. These quantities are difficult to isolate experimentally because (i) when the critical thickness is the larger of the two, the limiting thickness will inhibit its measurement and (ii) even when the opposite is true, because of limited nucleation kinetics, the amorphous film may still persist above the critical thickness, and the limiting thickness may again obstruct its direct observation.⁴⁴ To overcome this challenge, Reichel et al.⁴⁴ exposed {111}, {100}, and {110} Al single crystals to oxygen at temperatures ranging from 350 to 650 K to form ultrathin stoichiometric amorphous surface oxides and subsequently annealed them at a higher temperature under ultrahigh vacuum to test the thermodynamic stability of the films. For the (111) Al substrate, they were able to show that amorphous Al_2O_3 surface overgrowths are thermodynamically stable up to ~ 0.9 nm, in excellent agreement with the present ab initio prediction in Figure 5.

Here, we focused on oxide growth on the most dominant surface family in aluminum, that is, {111}. Given the agreement between the present ab initio calculations and earlier thermodynamic models²⁷ as well as the subsequent experiments,^{35,44} we expect ab initio simulations for the substrate–film configurations of minority Al surfaces such as {110} and {100} to yield similar critical thicknesses as in those models and experiments. Furthermore, it is important to note that the relative energetic stabilities here are calculated with DFT and therefore pertain only to low to moderate temperatures. The thermodynamic models presented by Jeurgens et al.²⁶ and Reichel et al.²⁷ include approximations for the entropic contributions for bulk, surface, or interface free energies, which yield a weakly increasing temperature dependence for

the critical thickness of the thermodynamic stability of amorphous alumina on various Al planes. The enthalpic contribution to the free energies as derived from DFT, therefore, provides a sufficiently accurate approximation for the critical amorphous film thickness up to moderately high temperatures (< 1000 K) in the oxidation of Al.

Overall, the analysis here represents, to the best of our knowledge, the first full ab initio assessment of amorphous versus crystalline polymorph selection on a substrate and provides evidence that the amorphous alumina indeed becomes thermodynamically stable at finite length scales as the passivation layer on aluminum is forming upon oxidation. In other words, crystallization of the amorphous passivation film is thermodynamically prohibited until the film thickness reaches above ~ 1 nm, and therefore the amorphous film can preserve its conformational coverage indefinitely under such conditions. We also found γ films at this length scale to be “amorphous-like” because of structural distortions. At higher temperatures where the film thickness increases, the limiting behavior of the films is known to vanish, and crystallization into γ and then to α -alumina (through several other intermediate phases) becomes inevitable, where the effectiveness in oxidation protection varies depending on the stable crystal phase, morphology, and microstructure.⁴⁹

Finally, stabilization of metastable phases, crystalline or amorphous, has long been addressed with alternative synthesis methods including but not limited to quenching, alloying, nanoparticle formation, and thin-film growth on a substrate, with examples not only in Al_2O_3 but also in many other polymorphic systems such as ZrO_2 , TiO_2 , GaN, and more.^{52–54} Although we have focused on the morphology of aluminum metal surface passivation, the ab initio framework we present is broadly applicable in the context of selection and stabilization of metastable polymorphs in the thin-film growth, especially in competition with the amorphous form as frequently encountered in synthesis.

4. CONCLUSIONS

Here, we presented an ab initio investigation of the thermodynamics of phase selection in passive film formation in aluminum. We showed that combining AIMD and DFT, realistic models of amorphous-film/crystalline-substrate and crystalline-film/crystalline-substrate configurations can be obtained, and relative stabilities of the film–substrate configurations can be calculated as a function of film thickness. We found that $\gamma\text{-Al}_2\text{O}_3$ becomes more stable than the corundum and amorphous polymorphs for film thicknesses down to ~ 1 nm, below which the amorphous film becomes more stable. In fact, $\gamma\text{-Al}_2\text{O}_3$ films lose all sixfold coordination and become mostly “amorphous-like” with four- and fivefold coordination-dominated local environments for Al. The approach presented here can be used for computational design and discovery of new corrosion-resistant alloys and semiconductors, by providing a first-principles framework to search for ways to induce a stable amorphous passivation layer. Other possible applications are expected to be in the area of thin-film deposition, in particular, searching for predictive pathways for polymorph selection during synthesis.

■ AUTHOR INFORMATION

Corresponding Author

*E-mail: kapersson@lbl.gov.

ORCID 

Muratahan Aykol: 0000-0001-6433-7217

Present Address

[§]Toyota Research Institute, Los Altos, CA 94022, USA (M.A.).

Notes

The authors declare no competing financial interest.

■ ACKNOWLEDGMENTS

This work was supported as part of the Computational Materials Sciences Program funded by the U.S. Department of Energy, Office of Science, Basic Energy Sciences, Materials Sciences and Engineering Division, award no. DE-SC0014607. This research used resources of the National Energy Research Scientific Computing Center, a DOE Office of Science User Facility supported by the Office of Science of the U.S. Department of Energy under contract no. DE-AC02-05CH1123.

■ REFERENCES

- (1) Macdonald, D. D. On the Existence of Our Metals-Based Civilization. *J. Electrochem. Soc.* **2006**, *153*, B213.
- (2) Macdonald, D. D. Passivity—the Key to Our Metals-Based Civilization. *Pure Appl. Chem.* **1999**, *71*, 951–978.
- (3) Macdonald, D. D.; Urquidi-Macdonald, M. Theory of Steady-State Passive Films. *J. Electrochem. Soc.* **1990**, *137*, 2395–2402.
- (4) Schultze, J. W.; Lohrengel, M. M. Stability, Reactivity and Breakdown of Passive Films. Problems of Recent and Future Research. *Electrochim. Acta* **2000**, *45*, 2499–2513.
- (5) Gulbransen, E. A.; Wysong, W. S. Thin Oxide Films on Aluminum. *J. Phys. Colloid Chem.* **1947**, *51*, 1087–1103.
- (6) Doherty, P. E.; Davis, R. S. Direct Observation of the Oxidation of Aluminum Single-Crystal Surfaces. *J. Appl. Phys.* **1963**, *34*, 619–628.
- (7) Fehlnner, F. P.; Mott, N. F. Low-Temperature Oxidation. *Oxid. Met.* **1970**, *2*, 59–99.
- (8) McBee, C. L.; Kruger, J. Nature of Passive Films on Iron-Chromium Alloys. *Electrochim. Acta* **1972**, *17*, 1337–1341.
- (9) Okamoto, G. Passive Film of 18-8 Stainless Steel Structure and Its Function. *Corros. Sci.* **1973**, *13*, 471–489.
- (10) Revesz, A. G.; Fehlnner, F. P. The Role of Noncrystalline Films in the Oxidation and Corrosion of Metals. *Oxid. Met.* **1981**, *15*, 297–321.
- (11) Fehlnner, F. P. Low Temperature Oxidation of Metals and Semiconductors. *J. Electrochem. Soc.* **1984**, *131*, 1645.
- (12) Kruger, J. The Nature of the Passive Film on Iron and Ferrous Alloys. *Corros. Sci.* **1989**, *29*, 149–162.
- (13) Ryan, M. P.; Newman, R. C.; Thompson, G. E. Atomically Resolved STM of Oxide Film Structures on Fe-Cr Alloys during Passivation in Sulfuric Acid Solution. *J. Electrochem. Soc.* **1994**, *141*, L164–L165.
- (14) Ryan, M. P.; Newman, R. C.; Thompson, G. E. A Scanning Tunneling Microscopy Study of Structure and Structural Relaxation in Passive Oxide Films on Fe-Cr Alloys. *Philos. Mag. B* **1994**, *70*, 241–251.
- (15) Ryan, M. R.; Newman, R. C.; Thompson, G. E. An STM Study of the Passive Film Formed on Iron in Borate Buffer Solution. *J. Electrochem. Soc.* **1995**, *142*, L177–L179.
- (16) Davenport, A. J.; Ryan, M. P.; Simmonds, M. C.; Ernst, P.; Newman, R. C.; Sutton, S. R.; Colligon, J. S. In Situ Synchrotron X-Ray Microprobe Studies of Passivation Thresholds in Fe-Cr Alloys. *J. Electrochem. Soc.* **2001**, *148*, B217–B221.
- (17) Jeurgens, L. P. H.; Sloof, W. G.; Tichelaar, F. D.; Mittermeijer, E. J. Structure and Morphology of Aluminium-Oxide Films Formed by Thermal Oxidation of Aluminium. *Thin Solid Films* **2002**, *418*, 89–101.
- (18) van Beek, H. J.; Mittermeijer, E. J. Amorphous and Crystalline Oxides on Aluminium. *Thin Solid Films* **1984**, *122*, 131–151.
- (19) Campbell, T.; Kalia, R. K.; Nakano, A.; Vashishta, P.; Ogata, S.; Rodgers, S. Dynamics of Oxidation of Aluminum Nanoclusters Using Variable Charge Molecular-Dynamics Simulations on Parallel Computers. *Phys. Rev. Lett.* **1999**, *82*, 4866–4869.
- (20) Campbell, T. J.; Aral, G.; Ogata, S.; Kalia, R. K.; Nakano, A.; Vashishta, P. Oxidation of Aluminum Nanoclusters. *Phys. Rev. B* **2005**, *71*, 205413.
- (21) Hasnaoui, A.; Politano, O.; Salazar, J. M.; Aral, G.; Kalia, R. K.; Nakano, A.; Vashishta, P. Molecular Dynamics Simulations of the Nano-Scale Room-Temperature Oxidation of Aluminum Single Crystals. *Surf. Sci.* **2005**, *579*, 47–57.
- (22) Fehlnner, F. P. Low-Temperature Oxidation. *Philos. Mag. B* **1987**, *55*, 633–636.
- (23) Sabioni, A. C. S.; Huntz, A. M.; Millot, F.; Monty, C. Self-Diffusion in Cr₂O₃III. Chromium and Oxygen Grain-Boundary Diffusion in Polycrystals. *Philos. Mag. A* **1992**, *66*, 361–374.
- (24) Heuer, A. H. Oxygen and Aluminum Diffusion in α -Al₂O₃: How Much Do We Really Understand? *J. Eur. Ceram. Soc.* **2008**, *28*, 1495–1507.
- (25) Pilling, N. B.; Bedworth, R. E. The Oxidation of Metals at High Temperatures. *J. Inst. Met.* **1923**, *29*, 529–582.
- (26) Jeurgens, L.; Sloof, W.; Tichelaar, F.; Mittermeijer, E. Thermodynamic Stability of Amorphous Oxide Films on Metals: Application to Aluminum Oxide Films on Aluminum Substrates. *Phys. Rev. B* **2000**, *62*, 4707–4719.
- (27) Reichel, F.; Jeurgens, L. P. H.; Mittermeijer, E. J. The Thermodynamic Stability of Amorphous Oxide Overgrowths on Metals. *Acta Mater.* **2008**, *56*, 659–674.
- (28) Lamparter, P.; Kniep, R. Structure of Amorphous Al₂O₃. *Phys. B* **1997**, *234–236*, 405–406.
- (29) Siegel, D. J.; Hector, L. G.; Adams, J. B. Adhesion, Atomic Structure, and Bonding at the Al(111)/ α -Al₂O₃(0001) Interface: A First Principles Study. *Phys. Rev. B* **2002**, *65*, 085415.
- (30) Jain, A.; Ong, S. P.; Hautier, G.; Chen, W.; Richards, W. D.; Dacek, S.; Cholia, S.; Gunter, D.; Skinner, D.; Ceder, G.; Persson, K. A. Commentary: The Materials Project: A Materials Genome Approach to Accelerating Materials Innovation. *APL Mater.* **2013**, *1*, 011002.
- (31) Siegel, D. J.; Hector, L. G.; Adams, J. B. Ab Initio Study of Al-Ceramic Interfacial Adhesion. *Phys. Rev. B* **2003**, *67*, 092105.
- (32) Sun, M.; Nelson, A. E.; Adjaye, J. Examination of Spinel and Nonspinel Structural Models for γ -Al₂O₃ by DFT and Rietveld Refinement Simulations. *J. Phys. Chem. B* **2006**, *110*, 2310–2317.
- (33) Wolverton, C.; Hass, K. C. Phase Stability and Structure of Spinel-Based Transition Aluminas. *Phys. Rev. B* **2000**, *63*, 024102.
- (34) Pinto, H. P.; Nieminen, R. M.; Elliott, S. D. Ab Initio Study of γ -Al₂O₃ Surfaces. *Phys. Rev. B* **2004**, *70*, 125402.
- (35) Reichel, F.; Jeurgens, L. P. H.; Richter, G.; van Aken, P. A.; Mittermeijer, E. J. The Origin of High-Mismatch Orientation Relationships for Ultra-Thin Oxide Overgrowths. *Acta Mater.* **2007**, *55*, 6027–6037.
- (36) Kresse, G.; Furthmüller, J. Efficiency of Ab-Initio Total Energy Calculations for Metals and Semiconductors Using a Plane-Wave Basis Set. *Comput. Mater. Sci.* **1996**, *6*, 15–50.
- (37) Kresse, G.; Furthmüller, J. Efficient Iterative Schemes for Ab Initio Total-Energy Calculations Using a Plane-Wave Basis Set. *Phys. Rev. B* **1996**, *54*, 11169.
- (38) Perdew, J. P.; Burke, K.; Ernzerhof, M. Generalized Gradient Approximation Made Simple. *Phys. Rev. Lett.* **1996**, *77*, 3865–3868.
- (39) Blöchl, P. E. Projector Augmented-Wave Method. *Phys. Rev. B* **1994**, *50*, 17953.
- (40) Ong, S. P.; Richards, W. D.; Jain, A.; Hautier, G.; Kocher, M.; Cholia, S.; Gunter, D.; Chevrier, V. L.; Persson, K. A.; Ceder, G. Python Materials Genomics (Pymatgen): A Robust, Open-Source Python Library for Materials Analysis. *Comput. Mater. Sci.* **2013**, *68*, 314–319.
- (41) Jain, A.; Ong, S. P.; Chen, W.; Medasani, B.; Qu, X.; Kocher, M.; Brafman, M.; Petretto, G.; Rignanese, G.-M.; Hautier, G.; Gunter, D.; Persson, K. A. FireWorks: A Dynamic Workflow System Designed for

High-Throughput Applications. *Concurrency Comput. Pract. Ex.* **2015**, *27*, 5037–5059.

(42) Mathew, K.; Montoya, J. H.; Faghaninia, A.; Dwarakanath, S.; Aykol, M.; Tang, H.; Chu, I.-h.; Smidt, T.; Bocklund, B.; Horton, M.; Dagdelen, J.; Wood, B.; Liu, Z.-K.; Neaton, J.; Ong, S. P.; Persson, K.; Jain, A. Atomate: A High-Level Interface to Generate, Execute, and Analyze Computational Materials Science Workflows. *Comput. Mater. Sci.* **2017**, *139*, 140–152.

(43) Momma, K.; Izumi, F. VESTA 3 for Three-Dimensional Visualization of Crystal, Volumetric and Morphology Data. *J. Appl. Crystallogr.* **2011**, *44*, 1272–1276.

(44) Reichel, F.; Jeurgens, L. P. H.; Richter, G.; Mittemeijer, E. J. Amorphous versus Crystalline State for Ultrathin Al₂O₃ Overgrowths on Al Substrates. *J. Appl. Phys.* **2008**, *103*, 093515.

(45) Kresse, G.; Schmid, M.; Napetschnig, E.; Shishkin, M.; Köhler, L.; Varga, P. Structure of the Ultrathin Aluminum Oxide Film on NiAl(110). *Science* **2005**, *308*, 1440–1442.

(46) Wagman, D. D.; Evans, W. H.; Parker, V. B.; Schumm, R. H.; Halow, I.; Bailey, S. M.; Churney, K. L.; Nuttall, R. L.. The NBS Tables of Chemical Thermodynamic Properties. *J. Phys. Chem. Ref. Data* **1982**, *11*, 127.

(47) Gutiérrez, G.; Johansson, B. Molecular Dynamics Study of Structural Properties of Amorphous Al₂O₃. *Phys. Rev. B* **2002**, *65*, 104202.

(48) Baran, J. D.; Grönbeck, H.; Hellman, A. Mechanism for Limiting Thickness of Thin Oxide Films on Aluminum. *Phys. Rev. Lett.* **2014**, *112*, 146103.

(49) Trunov, M. A.; Schoenitz, M.; Zhu, X.; Dreizin, E. L. Effect of Polymorphic Phase Transformations in Al₂O₃ Film on Oxidation Kinetics of Aluminum Powders. *Combust. Flame* **2005**, *140*, 310–318.

(50) Cai, N.; Zhou, G.; Müller, K.; Starr, D. E. Tuning the Limiting Thickness of a Thin Oxide Layer on Al(111) with Oxygen Gas Pressure. *Phys. Rev. Lett.* **2011**, *107*, 035502.

(51) Jeurgens, L. P. H.; Sloof, W. G.; Tichelaar, F. D.; Mittemeijer, E. J. Growth Kinetics and Mechanisms of Aluminum-Oxide Films Formed by Thermal Oxidation of Aluminum. *J. Appl. Phys.* **2002**, *92*, 1649–1656.

(52) Shukla, S.; Seal, S. Mechanisms of Room Temperature Metastable Tetragonal Phase Stabilisation in Zirconia. *Int. Mater. Rev.* **2005**, *50*, 45–64.

(53) Ding, H.; Dwarakanath, S. S.; Garten, L.; Ndione, P.; Ginley, D.; Persson, K. A. Computational Approach for Epitaxial Polymorph Stabilization through Substrate Selection. *ACS Appl. Mater. Interfaces* **2016**, *8*, 13086–13093.

(54) Navrotsky, A. Energetics of Nanoparticle Oxides: Interplay between Surface Energy and Polymorphism. *Geochem. Trans.* **2003**, *4*, 34.